Supplementary Figures

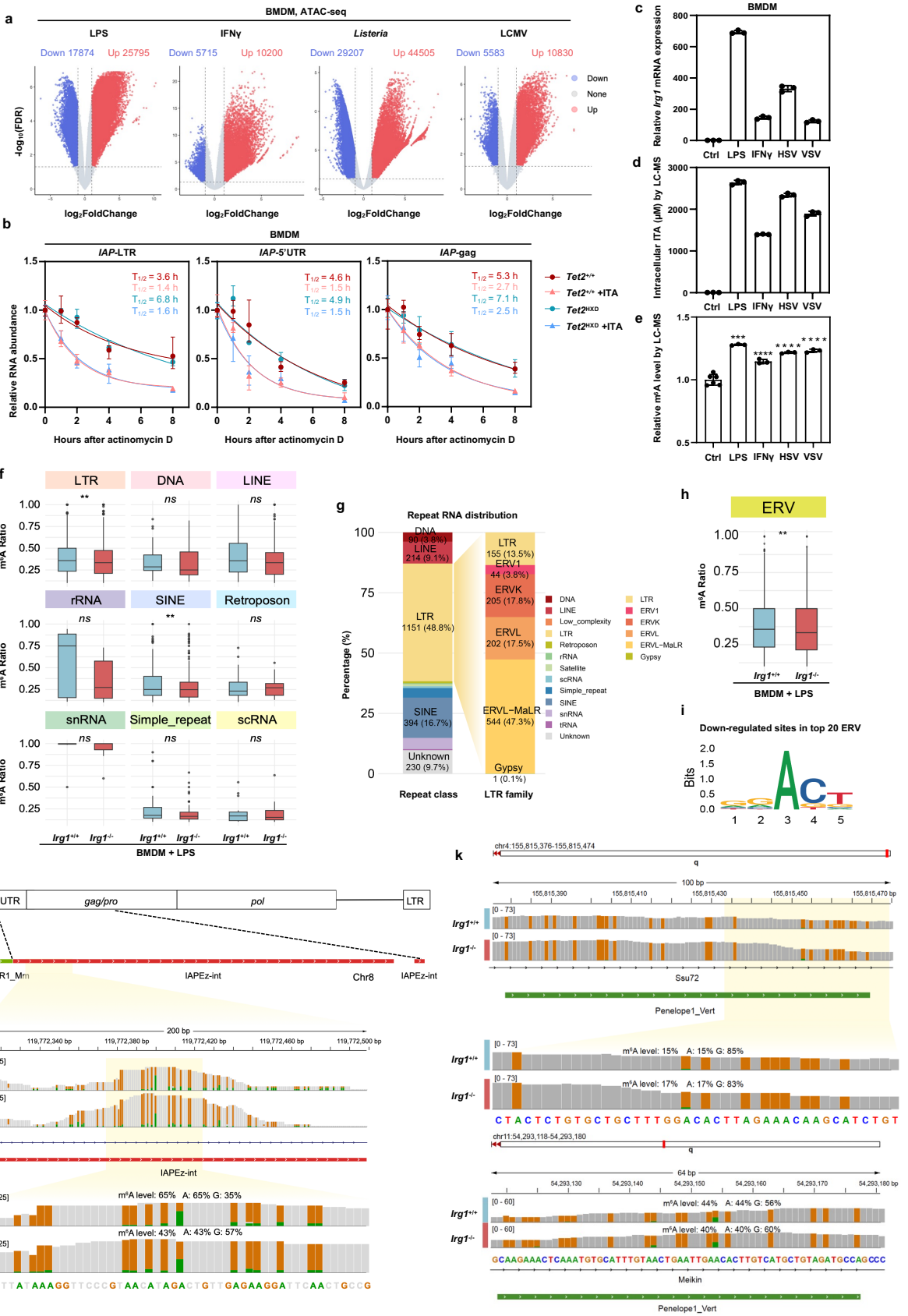

Supplementary Fig. S1 IRG1/ITA facilitates m^{6}A deposition on ERV transcripts during macrophage activation

(a) Volcano plots of ATAC-seq peaks (GSE263758) changes in BMDMs from wild-type mice treated with 24 hours stimulation by LPS, IFN-gamma, *Listeria monocytogenes* (*Listeria*) and lymphocytic choriomeningitis virus (LCMV). The x-axis represents $\log_2$ Foldchange, and the y-axis represents $-\log_{10}$(FDR). Differential peaks with fold change (FC) > 2 and FDR < 0.05 are indicated in red (up) and blue (down).

(b) ITA treatment reduces *IAP* mRNA stability in both *Tet2*$^{+/+}$ and *Tet2*^{HxD} BMDMs. BMDMs were pretreated with ITA (3 mM, 24 hours), and the stability of *IAP* transcripts was assessed in cells treated with actinomycin D (5 μg/mL) for 0, 1, 2, 4, or 8 hours. Transcript levels were normalized to 18S rRNA. Data present mean ± S.D. from four replicates. mRNA half-lives were calculated using a one-phase exponential decay model in GraphPad Prism.

(c) *Irg1* expression is induced by multiple inflammatory stimuli. BMDMs were stimulated with LPS (100 ng/mL), IFN-γ (20 ng/mL), VSV (MOI = 1), or HSV (MOI = 1) for 24 hours. The mRNA expression of *Irg1* was normalized to *Rps18*. Each data point represents an independent experiment.

(d) Multiple inflammatory stimuli induce ITA accumulation. BMDMs were stimulated as described in (c), and the intracellular concentrations of ITA were quantified by LC-MS/MS. Each data point represents an independent experiment.

(e) Inflammatory activation increases m^{6}A levels in macrophages. BMDMs were stimulated as described in (c), and total Poly(A)$^+$ RNA m^{6}A levels were quantified by LC–MS/MS. Each data point represents an independent experiment.

(f) Among reRNAs, LTRs display the most pronounced decrease in m^{6}A levels in *Irg1*$^{-/-}$ BMDMs after LPS stimulation. Boxplots depict changes in m^{6}A levels across reRNA categories.

(g) Repeat RNA composition is determined by GLORI-seq. Analysis of m^{6}A-modified repeat elements shows that ERVs constitute the major fraction within the LTR category.

(h) m^{6}A methylation of ERVs is reduced in *Irg1*$^{-/-}$ BMDMs after LPS stimulation. ERVs extracted from the LTR category in (f), exhibit decreased m^{6}A modification upon *Irg1* deletion.

(i) Motif analysis of down-regulated m^{6}A sites in the top 20 ERVs in *Irg1*$^{-/-}$ BMDMs after LPS stimulation, which are identified by GLORI-seq.

(j) Representative GLORI–seq tracks showing m^{6}A distribution at the 5′UTR region of *IAPEz* locus in WT and *Irg1*$^{-/-}$ BMDMs following LPS stimulation. Green and orange dots indicate methylated and unmethylated adenosines, respectively. The m^{6}A occupancy was decreased from 65% to 43% in WT and *Irg1*$^{-/-}$ cells, respectively.

(k) Representative GLORI–seq tracks showing m^{6}A distribution at *Penelope_Vert* locus in WT and *Irg1*$^{-/-}$ BMDMs following LPS stimulation. Green and orange dots indicate methylated and unmethylated adenosines, respectively, as described in (j).

Shown are average values with S.D. P values are calculated using two-tailed Student's t-test for paired comparisons. **denotes $p < 0.01$, ***denotes $p < 0.001$, and ****denotes $p < 0.0001$ for the indicated comparison.

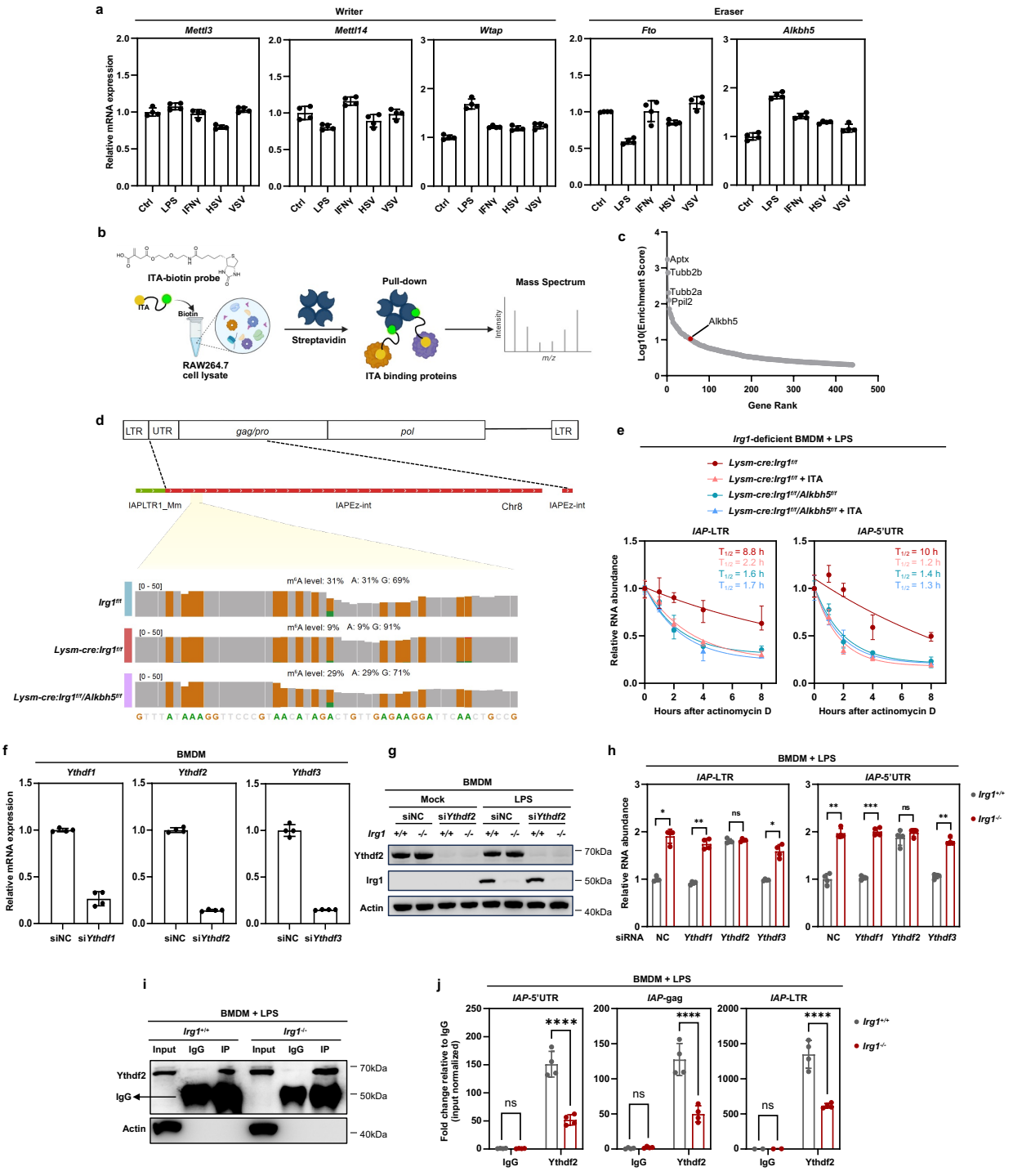

Supplementary Fig. S2 Itaconate binds to ALKBH5 and promotes YTHDF2-mediated ERV RNA decay

(a) mRNA expression of m^{6}A writers and erasers under various inflammatory stimuli. BMDMs were stimulated as indicated, and the transcript levels of *Mettl3*, *Mettl14*, *Wtap*, *Alkbh5*, and *Fto* were normalized to *Rps18*. Each data point represents an independent experiment.

(b) The ITA–biotin pull-down and mass spectrometry workflow is schematically illustrated. Cell lysates from RAW264.7 macrophages were incubated with ITA–biotin, followed by streptavidin-based enrichment. Bound proteins were analyzed by mass spectrometry to identify potential ITA-interacting candidate proteins.

(c) Proteomic analysis identifies Alkbh5 as an ITA-interacting protein. Following the ITA–biotin pull-down described in (b), mass spectrometry identified Alkbh5 among the top 50 enriched proteins, plotted as gene rank versus $\log_{10}$(enrichment score).

(d) Representative GLORI-seq tracks at the *IAPEz* locus (corresponding to the site shown in Supplementary Fig. S1j) in *Irg1*$^{f/f}$, *Lysm-cre:Irg1*$^{f/f}$, *Lysm-cre:Irg1*$^{f/f}$*/Alkbh5*$^{f/f}$(*Irg1*/*Alkbh5*-DKO) BMDMs stimulated with LPS (100 ng/mL) for 24 hours. Green and orange dots indicate methylated and unmethylated adenosines, respectively. m^{6}A occupancy at the indicated *IAPEz* site decreased from 31% in *Irg1*$^{f/f}$ BMDMs to 9% in *Irg1*-deficient BMDMs and was restored to 29% in *Irg1*/*Alkbh5*-DKO BMDMs.

(e) ITA decreases *IAP* RNA stability in an Alkbh5-dependent manner. BMDMs from *Lysm-cre:Irg1*$^{f/f}$ and *Lysm-cre:Irg1*$^{f/f}$*/Alkbh5*$^{f/f}$ mice were pretreated with ITA (3 mM, 3 hours) prior to LPS stimulation (100 ng/mL, 24 hours). Stability of indicated ERV transcripts was measured as described in (Fig. 2l).

(f-h) Knockdown of *Ythdf2* diminishes the difference in *IAP* RNA expression between *Irg1*$^{+/+}$ and *Irg1*$^{-/-}$ macrophages after LPS stimulation. In brief, BMDMs were transfected with siRNAs against *Ythdf1, Ythdf2*, or *Ythdf3*, and then challenged with LPS (100 ng/mL) for 24 hours. Knockdown efficiency of Ythdf2 was confirmed by western blotting. Actin served as the loading control (g). The mRNA expression of *Ythdf* genes and indicated *IAP* RNAs was determined by qRT-PCR, normalized to *Rps18* mRNA.

(i-j) *Irg1* deficiency impairs the association of Ythdf2 with *IAP* transcripts. BMDMs were stimulated with LPS (100 ng/mL) for 24 hours and subjected to RNA immunoprecipitation (RIP) using an anti-Ythdf2 antibody or control IgG. (i) Immunoblot analysis confirming Ythdf2 immunoprecipitation. (j) qRT–PCR analysis of the indicated *IAP* RNAs in Ythdf2 immunoprecipitates, presented as enrichment relative to IgG controls. Each dot represents an independent experiment.

Shown are average values with S.D. of four replicates. P values are calculated using two-way ANOVA for multiple comparisons. *denotes $p < 0.05$, **denotes $p < 0.01$, ***denotes $p < 0.001$, and ****denotes $p < 0.0001$ for the indicated comparison. n.s. = not significant.

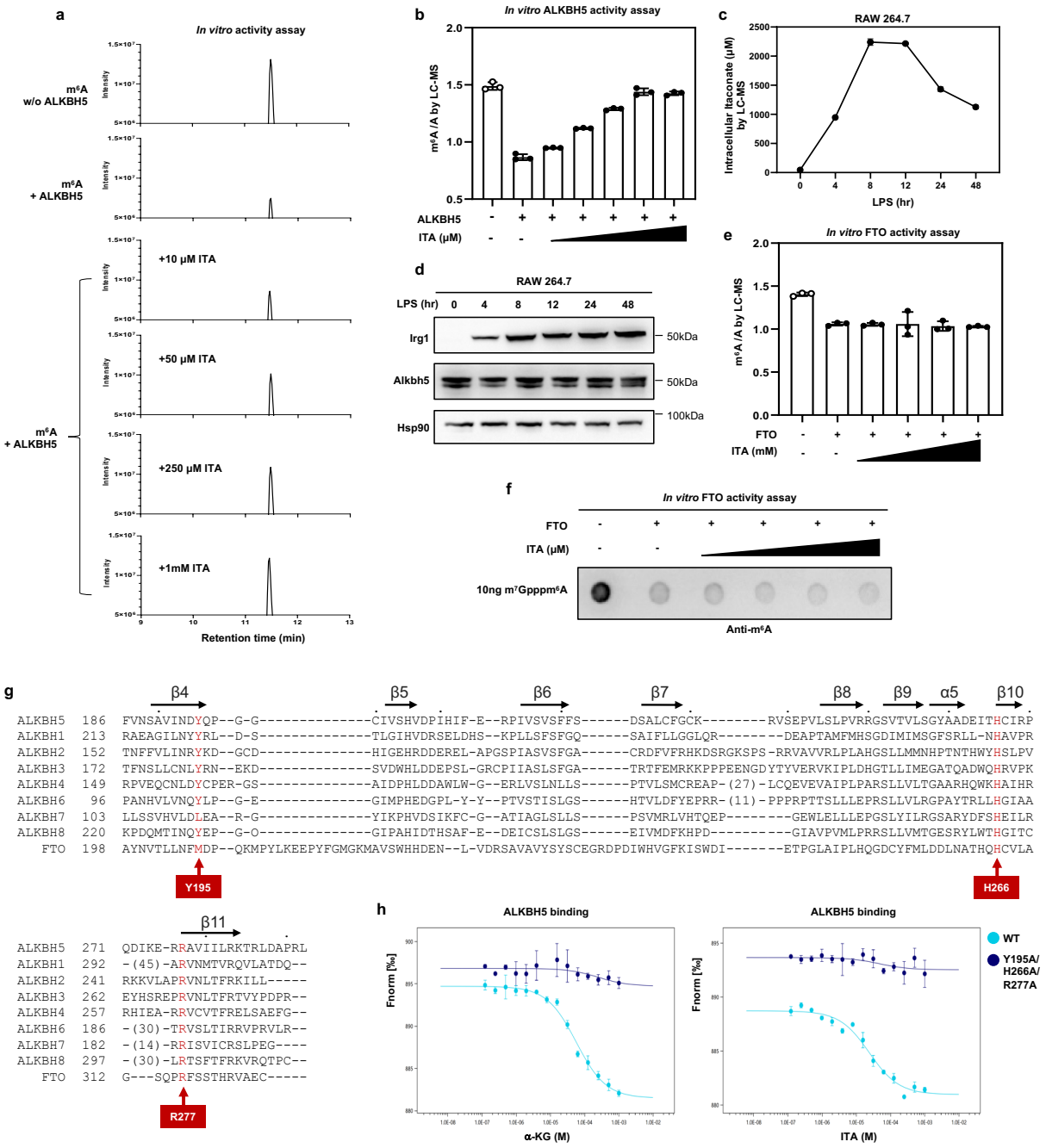

Supplementary Fig. S3 Itaconate inhibits the enzyme activity of ALKBH5, but not FTO

(a) Verification of residual m^{6}A levels by LC-MS/MS in demethylation reactions containing ALKBH5 and indicated doses of ITA.

(b) ITA inhibits ALKBH5 demethylase activity *in vitro*. Demethylation reactions were carried out in the presence of increasing doses of ITA (10, 20, 250, 1000, and 4000 μM). m^{6}A levels were quantified by LC–MS/MS and normalized to the total nucleoside content. Data present mean ± S.D. from three independent experiments.

(c) Intracellular ITA concentration in macrophages following LPS stimulation. RAW264.7 cells were stimulated with LPS (100 ng/mL) for the indicated durations, and intracellular ITA levels were measured by LC-MS/MS.

(d) LPS induced Irg1 protein expression without altering Alkbh5 protein levels. RAW264.7 cells were stimulated as described in (c), and protein levels of Irg1 and Alkbh5 were determined by western blot. Hsp90 served as a loading control.

(e-f) ITA does not inhibit FTO enzymatic activity. Demethylation reactions were carried out using ssRNA–m^6A (5'-AUUGUGG(m^6A)CUGCAG C-3') (e) or ssRNA –5'-m^7Gppp-m^6ACACUUGCUUUUGACACAACU-3' (f) as substrates in the presence of increasing doses of ITA. Residual m^6A was quantified by using dot-blot or LC-MS/MS, respectively.

(g) Residues H266 and R277 are strictly conserved across the ALKBH protein family. Y195 is also conserved in most ALKBH members, except for ALKBH7 and FTO. Sequence alignment was performed in accordance with the established sequences from the reference [29].

(h) Alanine substitution of key residues disrupts ITA and α-KG binding to ALKBH5. MST binding analysis was performed using purified wild-type or mutant ALKBH5 proteins with the indicated metabolites.

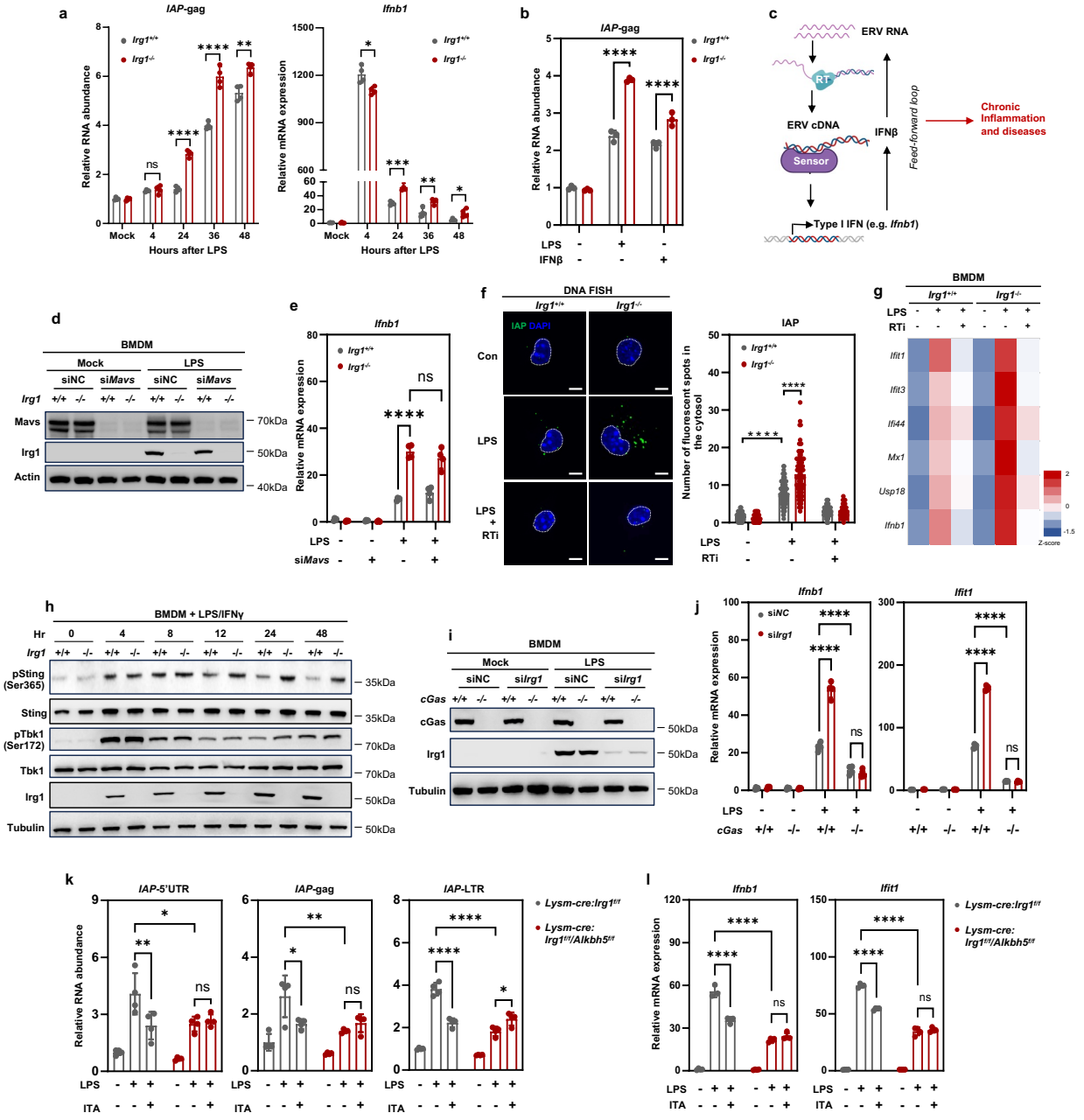

Supplementary Fig. S4 Itaconate-ALKBH5-ERV axis attenuates the cGAS/STING/IFN-I signaling pathway

(a) *Irg1*$^{-/-}$ BMDMs exhibit elevated expression of *IAP* and *Ifnb1* during the late stages of LPS stimulation. *Irg1*$^{-/-}$ versus *Irg1*$^{+/+}$ BMDMs were stimulated with LPS (100 ng/mL) for the indicated durations (0, 4, 24, 36, and 48 hours). Transcript levels of *IAP* and *Ifnb1* were determined by qRT-PCR and normalized to *Rps18* mRNA.

(b) Loss of *Irg1* enhances *IAP* expression upon LPS or IFNβ stimulation. BMDMs from *Irg1*$^{-/-}$ and *Irg1*$^{+/+}$ mice were stimulated with LPS (100 ng/mL, 24 hours) or IFNβ (200 ng/mL, 24 hours), and transcript level of *IAP* was quantified by qRT-PCR and normalized to *Rps18*.

(c) A proposed model of the feed-forward loop linking ERV reactivation, IFNβ production, and chronic inflammation.

(d-e) Knockdown of *Mavs* does not affect the elevated *Ifnb1* expression in *Irg1*-deficient macrophages after LPS challenge. In brief, *Irg1*$^{-/-}$ and *Irg1*$^{+/+}$ BMDMs were transfected with siRNA against *Mavs* and then stimulated with LPS (100 ng/mL) for 24 hours. Knockdown efficiency of Mavs was confirmed by western blotting. Actin was used as a loading control (d). The mRNA expression of *Ifnb1* was determined by qRT-PCR, normalized to *Rps18* mRNA.

(f) Loss of *Irg1* promotes cytoplasmic accumulation of IAP DNA following LPS stimulation. *Irg1*$^{-/-}$ and *Irg1*$^{+/+}$ BMDMs were treated with LPS (100 ng/mL, 24 hours) with or without RT inhibitors (RTi; 5 μM tenofovir and emtricitabine). Cytoplasmic *IAP* DNA was detected by DNA-FISH (Left). Nuclei were counterstained with DAPI and nuclear peripheries are outlined in white. Scale bar, 5 μm. Quantification of cytoplasmic IAP DNA fluorescence intensity was performed using Fiji (Right). Each dot represents one cell.

(g) RTi treatment restores the elevated *Ifnb1* and *ISG* expression in *Irg1*$^{-/-}$ BMDMs. *Irg1*$^{-/-}$ versus *Irg1*$^{+/+}$ BMDMs were pretreated with RTi (5 μM, 3 hours), followed by LPS stimulation (100 ng/mL, 24 hours). The mRNA expression of *Ifnb1* and selected ISGs was analyzed by qRT-PCR and visualized as heatmaps.

(h) Enhanced phosphorylation of Sting and Tbk1 in *Irg1*$^{-/-}$ BMDMs during the late stages of LPS stimulation. *Irg1*$^{-/-}$ and *Irg1*$^{+/+}$ BMDMs were stimulated with LPS (100 ng/mL) and IFN-γ (20 ng/mL) for the indicated durations. Phosphorylated Sting (p-Sting) and phosphorylated Tbk1 (p-Tbk1) were detected by western-blot analysis. Total Sting, Tbk1, and Tubulin served as loading controls.

(i) Western-blot analysis using the indicated specific antibodies validated *cGas* knockout and siRNA-mediated *Irg1* knockdown in BMDMs.

(j) Loss of *Irg1* augments LPS-induced *Ifnb1* and *Ifit1* expression in a cGas-dependent manner. *cGas*$^{+/+}$ and *cGas*$^{-/-}$ BMDMs were transfected with control (NC) or *Irg1*-targeting siRNA, followed by LPS stimulation (100 ng/mL, 24 hours). *Ifnb1* and *Ifit1* mRNA expression was quantified by qRT–PCR, normalized to *Rps18* mRNA. Each data point represents an independent experiment.

(k-l) Exogenous ITA suppresses *IAP* and IFN responses in an ALKBH5-dependent manner. BMDMs from *Lysm-cre:Irg1*$^{f/f}$ and *Lysm-cre:Irg1*$^{f/f}$*/Alkbh5*$^{f/f}$ mice were pretreated with ITA (3 mM, 3 hours) and stimulated with LPS (100 ng/mL, 24 hours). The mRNA expression of *IAP* and indicated genes was quantified by qRT-PCR and normalized to *Rps18* mRNA.

Shown are average values with S.D. of four replicates. P values are calculated using two-way ANOVA for multiple comparisons. *denotes $p < 0.05$, **denotes $p < 0.01$, and ****denotes $p < 0.0001$ for the indicated comparison. n.s. = not significant.

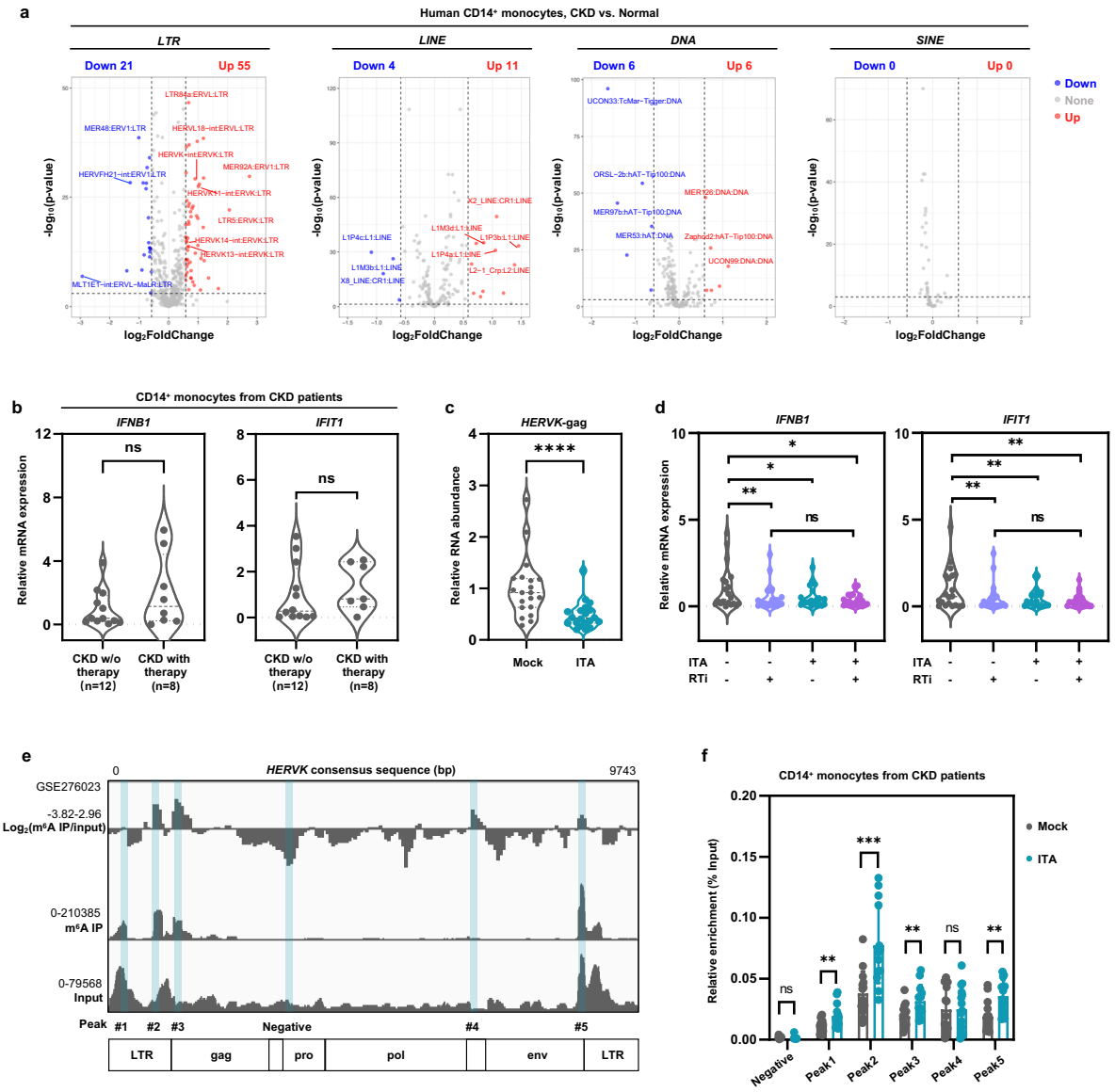

Supplementary Fig. S5 Itaconate restricts ERV activation and interferon responses in monocytes from CKD patients

(a) ERV families are upregulated in circulating CD14⁺ monocytes from CKD patients. Ribo-minus RNA-seq analysis of circulating CD14⁺ monocytes from CKD patients (n = 10) and healthy controls (n = 6). Volcano plots showing differentially expressed repeat elements of the indicated classes between CKD patients and healthy controls. The x-axis represents $\log_2$fold change, and the y-axis represents $-\log_{10}$ (P-value). Differentially expressed transposable elements with fold change (FC) > 1.5 and P < 0.001 are indicated in red (upregulated) and blue (downregulated).

(b) CD14⁺ monocytes were isolated from treatment-naïve CKD patients (n = 12) and those receiving RAS or/and SGLT-2 inhibitor therapy (n = 8), and subsequently subjected to qRT–PCR analysis. Transcript levels of *IFNB1* and *IFIT1* were normalized to *RPS18*. Each data point represents an individual donor.

(c) *In vitro* ITA treatment suppresses *HERVK* expression in peripheral monocytes from CKD patients. $CD14^+$ monocytes were treated with ITA (3 mM, 24 hours). *HERVK* expression was measured by qRT–PCR and normalized to *RPS18*. Each data point represents an individual donor.

(d) *In vitro* ITA or RTi treatment reduces *IFNB1* and *IFIT1* expression in peripheral monocytes from CKD patients. Cells were treated with ITA (3 mM) or RT inhibitors (5 μM) for 24 hours. Transcript levels of *IFNB1* and *IFIT1* were measured by qRT–PCR and normalized to *RPS18*. Each data point represents an individual donor.

(e) m^6A enrichment across *HERVK* transcripts. Genome browser tracks showing Input, m^6A-IP, and $\log_2$(IP/Input) signals mapped to the *HERVK* consensus sequence. Gray boxes indicate regions selected for MeRIP–qPCR validation.

(f) ITA treatment increases m^6A modification of *HERVK* transcripts in $CD14^+$ monocytes from CKD patients. $CD14^+$ monocytes were treated with ITA (3 mM) for 24 hours. m^6A enrichment on *HERVK* transcripts was quantified by MeRIP–qPCR using the primer sets shown in (e) and normalized to input. Each dot represents an individual donor.

Shown are average values with S.D. P values are calculated using two-tailed Student's t-test for paired comparisons or two-way ANOVA for multiple comparisons. *denotes $p < 0.05$, **denotes $p < 0.01$, ***denotes $p < 0.001$, and ****denotes $p < 0.0001$ for the indicated comparison. n.s. = not significant.

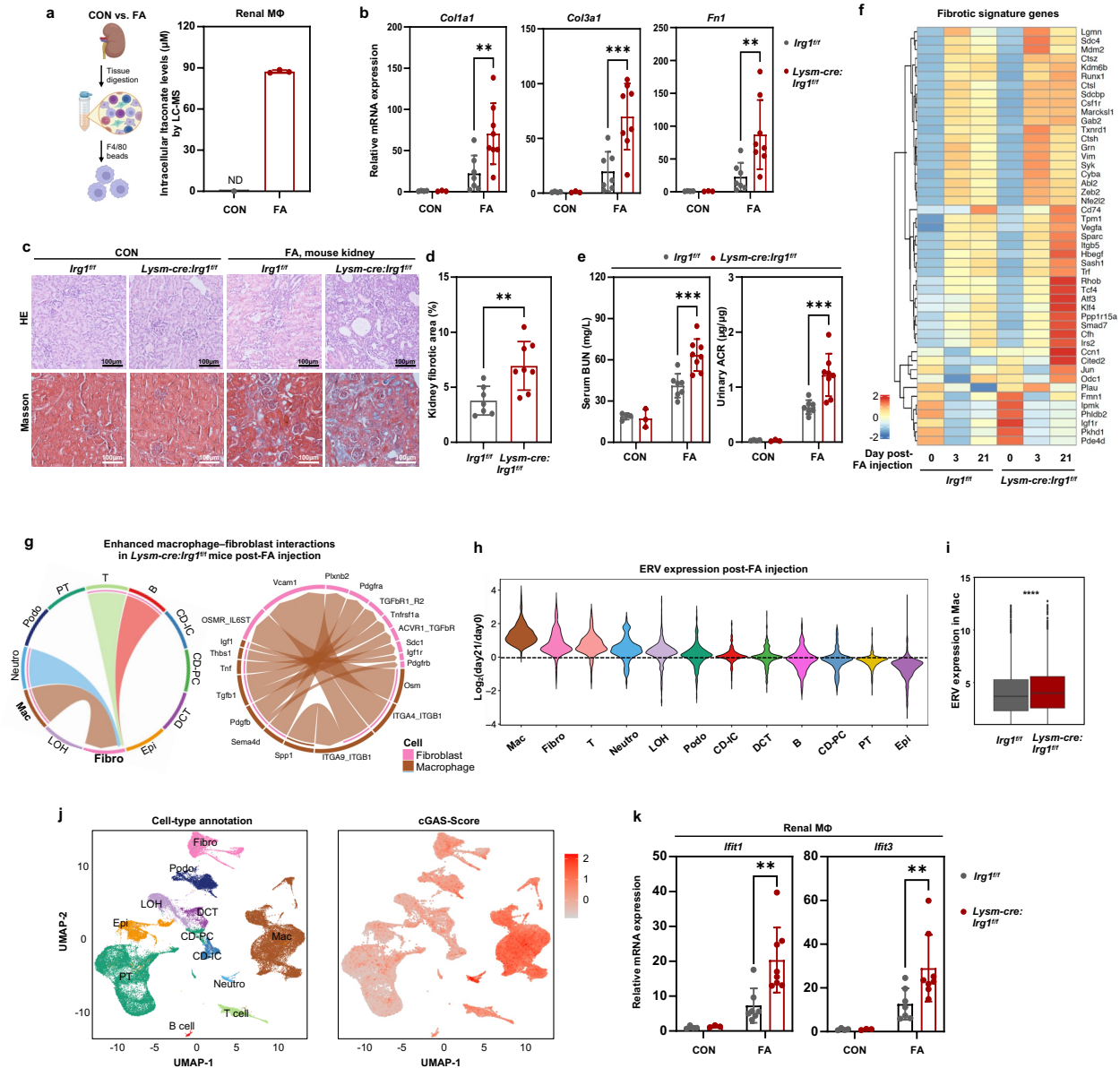

Supplementary Fig. S6 Loss of *Irg1* promotes ERV expression and exacerbates renal fibrosis

(a) ITA levels in renal macrophages are increased after FA injection. (Left) schematic workflow showing kidney harvesting, enzymatic dissociation, and magnetic enrichment of renal macrophages using anti-F4/80 microbeads (for details, see Methods). (Right) Intracellular ITA concentration in isolated renal macrophages, as determined by LC-MS/MS. ND, not detected.

(b) Loss of *Irg1* enhances expression of fibrosis-associated genes following FA injection. Mice were intraperitoneally injected with FA (125 mg/kg), and kidney tissues were harvested at day 21 for qRT–PCR analysis. *Gapdh* was used as an internal control for normalization. Each data dot represents an individual mouse. Control groups: *Irg1*$^{f/f}$ (n = 4), *Lysm-cre:Irg1*$^{f/f}$ (n = 3); FA-treated groups: *Irg1*$^{f/f}$ (n = 7), *Lysm-cre:Irg1*$^{f/f}$ (n = 8).

(c-d) *Lysm-cre:Irg1*$^{f/f}$ mice exhibit more severe kidney injury and collagen deposition than *Irg1*$^{f/f}$ controls following FA injection. Kidney injury and collagen deposition were assessed by H&E and

Masson's trichrome staining. Fibrotic areas, based on Masson's trichrome staining, were quantified using Fiji software. Each data dot represents an individual mouse.

(e) Myeloid-specific *Irg1* deficiency worsens kidney functions after FA injection. Blood urea nitrogen (BUN) levels and urine albumin-to-creatinine ratio (UACR) were determined by commercial kit . Each point represents an individual mouse. Control groups, *Irg1*$^{f/f}$ (n = 4) and *Lysm-cre:Irg1*$^{f/f}$ (n = 3); FA-treated groups, *Irg1*$^{f/f}$ (n = 7), *Lysm-cre:Irg1*$^{f/f}$ (n = 8).

(f) Renal fibroblast of *Lysm-cre:Irg1*$^{f/f}$ mice exhibit augmented fibrotic signatures after FA injection. Single-cell RNA-seq was performed on kidneys of *Irg1*$^{f/f}$ and *Lysm-cre:Irg1*$^{f/f}$ mice at day 0, day 3, day 21 after FA-injection. Heatmap shows normalized expression of fibrotic genes in renal macrophages.

(g) Cell-cell communication analysis using CellChat. Left, predicted intercellular signaling toward fibroblasts inferred from other kidney cell types. Right, chord diagram depicting potentiated macrophage–fibroblast crosstalk in *Lysm-cre:Irg1*$^{f/f}$ mice compared with *Irg1*$^{f/f}$ controls at day 21 post FA-injection, mediated by profibrotic ligand–receptor interactions.

(h) Renal macrophages exhibit the most pronounced ERV upregulation among all analyzed cell types following FA treatment. Violin plot showing ERV expression changes across renal cell types in the FA-induced nephropathy model at day 21 relative to day 0.

(i) *Irg1* deficiency increases ERV expression in renal macrophages after FA treatment. Box plot showing ERV expression in renal macrophages from *Irg1*$^{f/f}$, *Lysm-cre:Irg1*$^{f/f}$ mice at day 21 after FA treatment.

(j) Single-cell analysis of cGAS-STING pathway activity across genotypes. UMAP plots display annotated cell types in *Irg1*$^{f/f}$ and *Lysm-cre:Irg1*$^{f/f}$ mice at day 0, day 3, day 21 after FA-injection (Left). UMAP visualization of single-cell transcriptomes, colored by cGAS-STING pathway activity score (red: high, gray: low) (Right). The score was computed using AddModuleScore in Seurat based on the expression of cGAS-STING pathway-related genes (see Methods).

(k) Isolation and analysis of renal macrophages following FA injection. Renal macrophages were isolated as described in (a). qRT–PCR analysis of *Ifit1* and *Ifit3* expression in isolated macrophages, normalized to *Gapdh*. Each data point represents an individual mouse.

Shown are average values with S.D. P values are calculated calculated using two-tailed Student's t-test for paired comparisons or two-way ANOVA for multiple comparisons. **denotes $p < 0.01$, ***denotes $p < 0.001$, and ****denotes $p < 0.0001$ for the indicated comparison. n.s. = not significant.

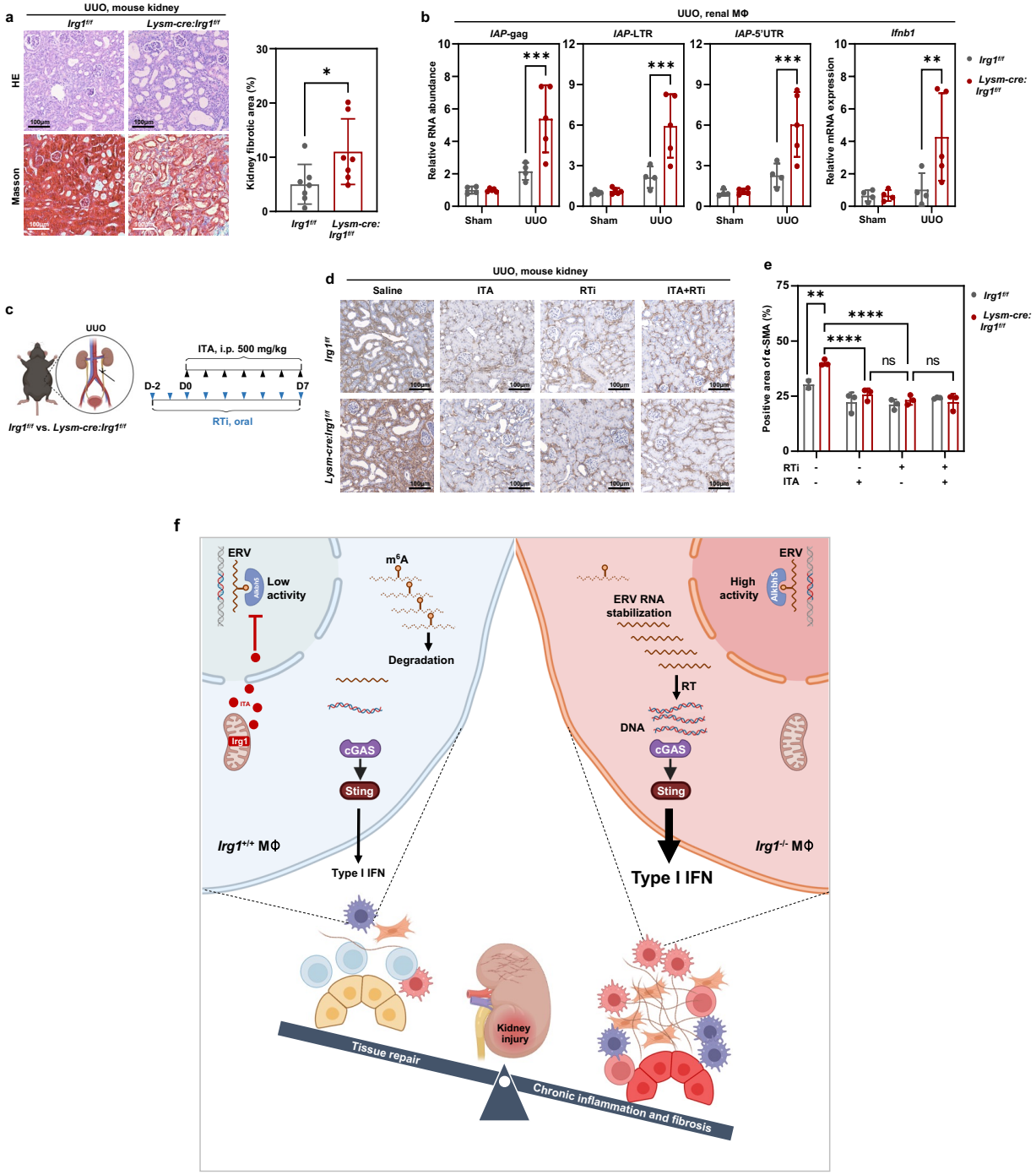

238

239

240 **Supplementary Fig. S7 Itaconate-mediated inhibition of ALKBH5 attenuates renal fibrosis by**
241 **suppressing ERVs**

242 **(a)** *Lysm-cre:Irg1*$^{f/f}$ mice exhibit more severe kidney injury and collagen deposition than *Irg1*$^{f/f}$
243 controls following UUO. Kidney injury and collagen deposition were assessed by H&E and
244 Masson's trichrome staining 7 days post-surgery. Fibrosis was quantified using Fiji software based

on Masson's trichrome staining. Each data point represents an individual mouse. (*Irg1*$^{f/f}$, n = 7; *Lysm-cre:Irg1*$^{f/f}$, n = 7).

(b) Increased expression of *IAP* and *Ifnb1* in renal macrophages from *Lysm-cre:Irg1*$^{f/f}$ mice following UUO. Renal macrophages were isolated from *Irg1*$^{f/f}$ and *Lysm-cre:Irg1*$^{f/f}$ mice seven days post-surgery. Transcript levels were quantified by qRT–PCR and normalized to *Gapdh*. Sham groups: *Irg1*$^{f/f}$ (n = 4) and *Lysm-cre:Irg1*$^{f/f}$ (n = 5); UUO groups: *Irg1*$^{f/f}$ (n = 4) and *Lysm-cre:Irg1*$^{f/f}$ (n = 5).

(c) Experimental schematic of ITA and/or RTi treatment in the UUO-induced nephrosis mouse model. In brief, *Irg1*$^{f/f}$ and *Lysm-cre:Irg1*$^{f/f}$ mice were treated with daily oral gavage of RT inhibitors (Tenofovir, 100 mg/kg; Emtricitabine, 60 mg/kg) starting two days prior to UUO surgery, and/or with intraperitoneal injection of ITA (500 mg/kg) initiated on the day of surgery.

(d-e) Combined ITA and RT inhibitor treatment does not provide additive protection against renal fibrosis in *Lysm-cre:Irg1*$^{f/f}$ mice following UUO. Briefly, *Irg1*$^{f/f}$ and *Lysm-cre:Irg1*$^{f/f}$ mice were treated as described in (c). Representative images of α-SMA immunohistochemical staining in the indicated groups are shown in (d), and α-SMA positive areas were quantified using Fiji software (e). Each data point represents an individual mouse.

(f) Schematic model depicting how ITA inhibits ALKBH5 to suppress endogenous retrovirus reactivation and chronic inflammation. In brief, activated macrophages undergo metabolic reprogramming that includes induction of IRG1 and synthesis of ITA. By competitively inhibiting ALKBH5 via α-KG displacement, ITA sustains m^{6}A methylation on ERV transcripts, ensuring their degradation. Consequently, *Irg1*-deficient macrophages fail to restrain ERVs, leading to their aberrant reactivation, chronic inflammation, and ultimately, the progression of renal fibrosis following injury.

Shown are average values with S.D. P values are calculated using two-tailed Student's t-test for paired comparisons or two-way ANOVA for multiple comparisons. *denotes $p < 0.05$, **denotes $p < 0.01$, ***denotes $p < 0.001$, and ****denotes $p < 0.0001$ for the indicated comparison. n.s. = not significant.

Supplementary Tables

Supplementary Table 1. Clinical characteristics of 23 cases of IgA nephropathy participants enrolled in this study

	CKD 1-2	**CKD 3**	**CKD 4-5**	***P***
	(n=11)	**(n=4)**	**(n=8)**	
Gender, n (%)				0.530
Male	3 (27.3%)	2 (50%)	4 (50%)	
Female	8 (72.7%)	2 (50%)	4 (50%)	
Age (years), median (IQR)	42 (24.0,49.0)	45.5 (38.25,59.5)	49.5 (34.0,67.5)	0.246
BMI (kg/m2), mean (SD)	22.8±4.0	25.6±5.2	25.7±4.4	0.333
SBP (mmHg), mean (SD)	123.9±18.3	124.3±5.9	132.1±14.4	0.244
DBP (mmHg), mean (SD)	80.1±9.9	82.0±4.1	89.0±10.0	0.099
Hb (g/L), mean (SD)	130.8±15.7	120.0±10.6	111.1±19.9	0.105
Cr (μmol/L), mean (SD)	69.2±15.5	135.3±18.9	334.6±229.3	<0.0001
UA (μmol/L), mean (SD)	276.7±70.9	359.3±49.1	457.5±130.8	0.008
BUN (mmol/L), mean (SD)	5.0±0.8	8.7±2.4	15.7±4.3	0.0001
FPG (mmol/L), mean (SD)	5.2±0.7	5.1±0.5	5.3±0.7	0.889
Albumin (g/L), mean (SD)	40.6±4.6	38.5±4.8	39.5±5.7	0.835
TG (mmol/L), mean (SD)	1.6±1.7	1.5±0.3	3.6±3.8	0.028
TC (mmol/L), mean (SD)	4.6±1.0	5.9±0.7	5.0±1.9	0.217
Renal pathology, n (%)				0.001
Lee I	0	0	0	
Lee II	1(9.1%)	0	0	
Lee III	8 (72.7%)	2 (50%)	1 (12.5%)	
Lee IV	2 (18.2%)	2 (50%)	1 (12.5%)	
Lee V	0	0	6(75.0%)	

BMI, body mass index; SBP, systolic blood pressure; DBP, diastolic blood pressure; Hb, hemoglobin; FPG, fast plasma glucose; TG, triglyceride; TC, total cholesterol; Cr, serum creatinine; UA, serum uric acid; BUN, blood urea nitrogen; IgAN, IgA nephropathy.

Supplementary Table 2. Clinical characteristics of 27 cases of CKD patients enrolled in this study

	CKD 1-2	**CKD 3**	**CKD 4-5**	***P***
	(n=11)	**(n=9)**	**(n=7)**	
Gender, n (%)				
Male	7 (63.6%)	7 (77.8%)	4 (57.1%)	
Female	4 (36.4%)	2 (22.2%)	3 (42.9%)	
Age (years), median (IQR)	51.0 (32.0, 57.0)	54.0 (28.5, 63.5)	49.0 (41.0, 61.0)	0.931
BMI (kg/m2), mean (SD)	25.8±4.4	23.6±5.2	24.9±3.2	0.686
Urine Protein (g/d), mean (SD)	2.4±2.2	1.0±1.7	2.4±2.1	0.084
Cr (μmol/L), mean (SD)	86.7±25.5	152.8±18.3	363.0±248.7	<0.0001
Renal pathology, n (%)				-
IgAN	5(45.5%)	2	3(42.9%)	
DN	1(9.1%)	1	1(14.3%)	
ANS	0	2	0	
FSGS	1(9.1%)	1	1(14.3%)	
LN	1(9.1%)	0	0	
Amyloidosis	1(9.1%)	0	0	
CIN	1(9.1%)	1	0	
Other	1(9.1%)	2	2(28.6%)	
RASi/SGLT2i	6 (54.5%)	5 (55.6%)	3 (42.9%)	>0.999

BMI, body mass index; Cr, serum creatinine; IgAN, IgA nephropathy; DN, diabetic nephropathy; ANS, arterionephrosclerosis; FSGS, focal segmental glomerulosclerosis; LN, lupus nephritis; CIN, chronic interstitial nephritis; RASi, renin-angiotensin system inhibitor; SGLT2i, sodium-glucose co-transporter 2 Inhibitor. Note: Macrophages derived from 20 of these patients were used to assess the interferon response (Supplementary Fig. S4a) and to undergo ITA and/or RTi treatment (Supplementary Fig. S4b-c).

Supplementary Table 3. Clinical characteristics of 10 cases of CKD participants enrolled in this analysis of ribominus RNA-seq

	Total(n=10)
Gender, n (%)	
Male	6 (60.0%)
Female	4 (40.0%)
Age (years), median (IQR)	53.2±9.4
BMI (kg/m2), mean (SD)	25.7±3.3
Urine Protein (g/d), mean (SD)	1.16(0.25,7.15)
Cr (μmol/L), mean (SD)	145.5±87.2
eGFR (ml/min/1.73m2), mean (SD)	56.0±27.1
CKD stage	
1-2	5(50.0%)
3	3(30.0%)
4-5	2(20.0%)
Renal pathology, n (%)	
IgAN	3(30.0%)
FSGS	4(40.0%)
DN	2(20.0%)
MN	1(10.0%)
RASi/SGLT2i	6 (60.0%)

BMI, body mass index; Cr, serum creatinine; eGFR, estimated glomerular filtration rate; CKD,chronic kidney disease; IgAN, IgA nephropathy; DN, diabetic nephropathy; FSGS, focal segmental glomerulosclerosis; MN, membranous nephropathy; RASi, renin-angiotensin system inhibitor; SGLT2i, sodium-glucose co-transporter 2 Inhibitor.

Supplementary Table 4. Clinical characteristics of 15 cases of CKD patients enrolled in the analysis of MeRIP–qPCR

	Total(n=15)
Gender, n (%)	
Male	10 (66.7%)
Female	5 (33.3%)
Age (years), median (IQR)	48.33±15.1
BMI (kg/m2), mean (SD)	27.2±5.9
Urine Protein (g/d), mean (SD)	2.57(0.83,3.63)
Cr (μmol/L), mean (SD)	120.5±62.2
eGFR (ml/min/1.73m2), mean (SD)	68.8±30.2
CKD stage	
1-2	8(53.4%)
3	5(33.3%)
4-5	2(13.3%)
Renal pathology, n (%)	
IgAN	5(33.3%)
FSGS	5(33.3%)
DN	1(6.7%)
MN	1(6.7%)
ANCA	1(6.7%)
LN	1(6.7%)
TIN	1(6.7%)
RASi/SGLT2i	8 (50.0%)

BMI, body mass index; Cr, serum creatinine; IgAN, IgA nephropathy; DN, diabetic nephropathy; FSGS, focal segmental glomerulosclerosis; MN, membranous nephropathy; ANCA, anti-neutrophil cytoplasmic antibodies-related nephritis; LN, lupus nephritis; TIN, tubule-interstitial nephritis; RASi, renin-angiotensin system inhibitor; SGLT2i, sodium-glucose co-transporter 2 Inhibitor.

Supplementary Table 5. Sequences of qRT-PCR, FISH primers and si-RNA used in this study

Gene	Sequence	Application	Species
Ifnb1-F	TCCGAGCAGAGATCTTCAGGAA	qRT-PCR	MUS
Ifnb1-R	TGCAACCACCACTCATTCTGAG	qRT-PCR	MUS
Ifit1-F	TACAGGCTGGAGTGTGCTGAGA	qRT-PCR	MUS
Ifit1-R	CTCCACTTTCAGAGCCTTCGCA	qRT-PCR	MUS
Ifit3-F	GCTCAGGCTTACGTTGACAAGG	qRT-PCR	MUS
Ifit3-R	CTTTAGGCGTGTCCATCCTTCC	qRT-PCR	MUS
Ifi44-F	CTGATTACAAAAGAAGACATGACAGAC	qRT-PCR	MUS
Ifi44-R	AGGCAAAACCAAAGACTCCA	qRT-PCR	MUS
Mx1-F	GACCATAGGGGTCTTGACCAA	qRT-PCR	MUS
Mx1-R	AGACTTGCTCTTTCTGAAAAGCC	qRT-PCR	MUS
Usp18-F	GAGAGGACCATGAAGAGGA	qRT-PCR	MUS
Usp18-R	TAAACCAACCAGACCATGAG	qRT-PCR	MUS
IAP-gag-F	AATCTCAGAACCGCTCCATGA	qRT-PCR	MUS
IAP-gag-R	TTTCTTAAAATGCCCAGGCTT T	qRT-PCR	MUS
IAP-5'UTR-F	CGGGTCGCGGTAATAAAGGT	qRT-PCR	MUS
IAP-5'UTR-R	ACTCTCGTTCCCCAGCTGAA	qRT-PCR	MUS
IAP-LTR-F	CGGGTCGCGGTAATAAAGGT	qRT-PCR	MUS
IAP-LTR-R	ACTCTCGTTCCCCAGCTGAA	qRT-PCR	MUS
Irg1-F	AAGTTTTCTGGCCTCGACCT	qRT-PCR	MUS
Irg1-R	CGTGGGAAACAGCAATAGCC	qRT-PCR	MUS
Mettl3-F	GAAACAGCTGGACTCGCTTC	qRT-PCR	MUS
Mettl3-R	GGCACGGGACTATCACTACG	qRT-PCR	MUS
Rn18S-F	CGCGGTTCTATTTTGTTGGT	qRT-PCR	MUS
Rn18S-R	AGTCGGCATCGTTTATGGTC	qRT-PCR	MUS
Mettl14-F	GCTAAGTCAAACACTCCTCCCA	qRT-PCR	MUS

Mettl14-R	TATTCTTCCAGAGGGGGCTC	qRT-PCR	MUS
Wtap-F	ATGGCACGGGATGAGTTAATTC	qRT-PCR	MUS
Wtap-R	TTCCCTTAAACCAGTCACATCG	qRT-PCR	MUS
Alkbh5-F	CGCGGTCATCAACGACTACC	qRT-PCR	MUS
Alkbh5-R	ATGGGCTTGAACTGGAACTTG	qRT-PCR	MUS
Fto-F	GACACTTGGCTTCCTTACCTG	qRT-PCR	MUS
Fto-R	CTCACCACGTCCCGAAACAA	qRT-PCR	MUS
Gapdh-F	TTTGATGTTAGTGGGGTCTCG	qRT-PCR	MUS
Gapdh-R	GTCCCGTAGACAAAATGGTGA	qRT-PCR	MUS
Rps18-F	TTCCAGCACATTTTGCGAGTA	qRT-PCR	MUS
Rps18-R	CACGCCCTTAATGGCAGTGAT	qRT-PCR	MUS
Fn1-F	ATGTGGACCCCTCCTGATAGT	qRT-PCR	MUS
Fn1-R	GCCCAGTGATTTCAGCAAAGG	qRT-PCR	MUS
Col1a1-F	GCTCCTCTTAGGGGCCACT	qRT-PCR	MUS
Col1a1-R	ATTGGGGACCCTTAGGCCAT	qRT-PCR	MUS
Col3a1-F	CTGTAACATGGAAACTGGGGAAA	qRT-PCR	MUS
Col3a1-R	CCATAGCTGAACTGAAAACCACC	qRT-PCR	MUS
HERVK-gag-F	AGCAGGTCAGGTGCCTGTAACATT	qRT-PCR	HOMO
HERVK-gag-R	TGGTGCCGTAGGATTAAGTCTCCT	qRT-PCR	HOMO
IFNB1-F	CTTGGATTCCTACAAAGAAGCAGC	qRT-PCR	HOMO
IFNB1-R	TCCTCCTTCTGGAACTGCTGCA	qRT-PCR	HOMO
IFIT1-F	GCCTTGCTGAAGTGTGGAGGAA	qRT-PCR	HOMO
IFIT1-R	ATCCAGGCGATAGGCAGAGATC	qRT-PCR	HOMO
HERVK-env-F	GGAGATGGTAACACCAGTCACAT	qRT-PCR	HOMO
HERVK-env-R	GGATAACGATACCCAATGGAAAT	qRT-PCR	HOMO
HERVK6-F	GCACTGATCCAACAGGAAAGGC	qRT-PCR	HOMO
HERVK6-R	TCTGCTCCAGTGTCTACCAACC	qRT-PCR	HOMO
RPS18-F	GCAGAATCCACGCCAGTACAAG	qRT-PCR	HOMO

RPS18-R	GCTTGTTGTCCAGACCATTGGC	qRT-PCR	HOMO
IRG1-F	TGGGGCCTTTTATGCCAACT	qRT-PCR	HOMO
IRG1-R	CTCACCTGTGGCCTGTTGAT	qRT-PCR	HOMO
IAP	TCCTTAGAAAGTTCAAGGCC	FISH	MUS
IAP	CTTGGAAAGGCCTGTATACT	FISH	MUS
IAP	CTGTTTCCTCAGAGGAGAAT	FISH	MUS
IAP	TATATTTGCCCATACTAGGG	FISH	MUS
IAP	CTTGTAAGCCTTTGTTCTTT	FISH	MUS
IAP	GGAAGAATTCTGCCCTTTAT	FISH	MUS
IAP	TATCTCAGGTCCTGCAAATT	FISH	MUS
IAP	TATACTTTTATCTGCTCCGG	FISH	MUS
IAP	GCCCAAATGCTGCATAATAT	FISH	MUS
IAP	CCCTTGGACACAAAGGTATA	FISH	MUS
IAP	CTTTATGGCACAGGAGGATG	FISH	MUS
IAP	GGGGAGGAGATATGAGGATC	FISH	MUS
IAP	TTTTAGCTGGGGATACGTTT	FISH	MUS
IAP	TGTTTGGATACCACTTTACC	FISH	MUS
IAP	TAACAATGTCACGGGCTTCT	FISH	MUS
IAP	AATACCGCGTGGGTTAATTC	FISH	MUS
IAP	CTGGCTCTGAACAATGACGT	FISH	MUS
IAP	TGTTAATGGTGTCAGTCGTC	FISH	MUS
IAP	TGACAAATTAGCTGCCCTAG	FISH	MUS
IAP	AATGAGACTAGCCTCGTGAG	FISH	MUS
Ythdf1	CCCGUAUCUCACUACCUAU	siRNA	MUS
Ythdf2	GCCGAATAATGCATATACT	siRNA	MUS
Ythdf3	GCGTTTGGATGCAGCTTAT	siRNA	MUS
Mavs	CAGAGAGCAUCAAGAGCAA	siRNA	MUS
Irg1	CAGGTTTACCAATATCTAATT	siRNA	MUS

IRG1	GCTGGCTTTCAATGTTGGTATTGAA	siRNA	HOMO
HERVK site1 f	ACAGATGCTTGAAGGCAGCATG	MeRIP–qPCR	HOMO
HERVK site1 r	GAAACCTTGGACAATACCTGGCT	MeRIP–qPCR	HOMO
HERVK site2 f	TGGCGGGATCCTCCATATGC	MeRIP–qPCR	HOMO
HERVK site2 r	TGGGTGTTTCTCGTAAGGTGGG	MeRIP–qPCR	HOMO
HERVK site3 f	ACAATTTTGCCCATGGTTTCCAGAAC	MeRIP–qPCR	HOMO
HERVK site3 r	GGCCCAATCATTCCATACTGTAAGTGG	MeRIP–qPCR	HOMO
HERVK site4 f	ACAAGATGAACAAAATGGTGACGTCAG	MeRIP–qPCR	HOMO
HERVK site4 r	GATATTTTGTAGCTAACTGCGTCAGCT	MeRIP–qPCR	HOMO
HERVK site5 f	ATCTCATATTAATCCTTGTGTGCCTGT	MeRIP–qPCR	HOMO
HERVK site5 r	ACAAAACCGCCATCGTCATCAT	MeRIP–qPCR	HOMO
HERVK negative f	CAGGGAATAAGCCAGTTACCACAA	MeRIP–qPCR	HOMO
HERVK negative r	CCTGGAAGCAGAGAGACTGCTT	MeRIP–qPCR	HOMO

311
312

Supplementary Table 6. Data collection and refinement statistics

Structure	**ALKBH5 (aa 71-298)**
PDB ID	9WL1
Data Collection	
Space group	$P4_32_12$
Cell dimensions	
a,b,c [Å]	56.80, 56.80, 146.56
α, β, γ [°]	90, 90, 90
Resolution [Å]	38.74-2.10 (2.16-2.10)[a]
Completeness [%]	99.7 (96.3)
R_{merge}[b]	0.081 (0.798)
Number unique	14754 (1125)
I/σI	23.8 (3.0)
CC1/2	1.000 (0.782)
Redundancy	21.5 (11.8)
Refinement	
Resolution (Å)	38.74-2.10
Reflections (working set)	14687
Reflections (test set)	764
No. atoms/B-factor ($Å^2$)	1889/41.90
Protein	1750/41.44
Water	117/45.52
R_{work}/R_{free}[c]	0.202/0.246
RMS deviations	
Bond lengths (Å)	0.009

Bond angles (°)	1.015
Ramachandran Plot % residues	
Favored	95.8%
Allowed	4.2%
Outliers	0

[a] Numbers in parentheses represent the highest resolution shell.

[b] Rmerge = ∑hkl∑i|Ii(hkl)−<I(hkl)>|/∑hkl∑iIi(hkl).

[c] R-factor = ∑hkl||Fo|−|Fc||/∑hkl|Fo|.